Characteristics of dynamically formed oxide films on molten aluminium

B. Nayebi and M. Divandari*

The characteristics of oxide films formed within a short time of pouring were investigated using samples prepared via the oxide–metal–oxide sandwich (OMO) technique. Surfaces of the OMO sandwiches were studied using scanning electron microscopy. The thickness of the folds of oxide films was examined and compared with previously obtained values for Al–7Si–0·4Mg and Al–5Mg alloys. Results showed that the thicknesses of oxide films formed in pure aluminium and Al-7Si-0.4Mg alloy are very close and in the range 100-500 nm.

Keywords: Aluminium oxide films, Short time oxidation, OMO sandwich, Fold, Wrinkle, Casting, Entrainment defects

Introduction

Most of researches on the oxidation of molten aluminium alloys has been carried out on stagnant melts and in long times. In the casting process, the molten metal is in motion, especially during pouring, and solidifies in a rather short time. According to reports on long time oxidation of stagnant molten aluminium, oxidation of the pure aluminium melt starts by the rapid formation of an amorphous alumina layer. After an initial incubation time, the amorphous alumina changes to crystalline γ alumina, slowing the rate of oxidation. After a further incubation period, the oxide structure converts to α alumina accompanied by a decrease in the volume of the oxide. Cracks can then form in the oxide layer, and combined with a higher mobility of the aluminium and oxygen ions in the α alumina, it can lead to a faster rate of oxidation and thus growth of surface oxide film.[1–4]

In casting condition, many parameters such as melt temperature, pouring time, chemical composition of the alloy, the environment in the mould and flow condition may affect the oxidation behaviour and rate of oxidation. With respect to these factors, the morphology of the surface oxide film and its thickness are different within a short time of pouring than in melts that have been stagnant for longer periods. This would suggest that investigation techniques on short time oxidation need to be different from those used in stagnant melt.

However, artificial bubbling of different atmospheres into the melt has been applied to study the oxidation of alloys under casting conditions.[5–9] Wightman and Fray, who entrained carbon dioxide bubbles into the molten aluminium, suggested that stagnant melt oxidation is ~60 times slower than oxidation under flow condition.[5]

Studies on the fracture surface of castings poured turbulently have confirmed the existence of oxide films. The oxides that are entrained into the melt during the filling of the mould (new oxide film) show a characteristic appearance, being observed to be thin and so finely folded when viewed in the scanning electron microscopy (SEM). Older films that form earlier during the melting process are thicker as deduced from their thicker folds (Fig. 1).[10–12]

Entrainment action necessarily occurs through a kind of folding process in which a double film, characterised by a dry surface to dry surface contact, is created, and therefore, it effectively constitutes a crack (Fig. 2). It should be noted that the entrainment action is a continuous process that occurs in milliseconds.[13,14] Furthermore, the entrapped air between two layers of double oxide films can act as a suitable site for gas and shrinkage porosity nucleation. The thickness of oxide films is a criterion of oxidation intensity that must be investigated morphologically.[15]

The oxide–metal–oxide (OMO) sandwich technique that has been introduced by one of the authors seems to have a good potential for the investigation of film formation characteristics, in very short times, in different alloys. This technique is based on introducing a steady succession of bubbles artificially and examining the adjacent bubbles' contact area by SEM. This technique could be used to make comparisons between the thickness and morphologies of the films in different film forming alloys and even to study the melt solidification behaviour.[15–18] Figure 3 shows an OMO sandwich of Al–5Mg alloy in which the nucleation site is quite visible, suggesting that the study of enucleating materials is possible using this technique.[16]

Previous works have been conducted on two industrial alloys, namely, Al–7Si–Mg and Al–5Mg. This research, which is in the line of the above mentioned investigations, was conducted based on the same technique to study and compare the morphology and thickness of commercially pure Al and two previously studied alloys.

Experimental

Pure commercial aluminium was melted at 760°C in an electrical resistance furnace under a commercially

School of Metallurgy and Materials Engineering, Iran University of Science and Technology (IUST), Narmak, Tehran, Iran

*Corresponding author, email divandari@iust.ac.ir

Received 2 December 2010; accepted 18 May 2012
DOI 10.1179/1743133612Y.0000000026

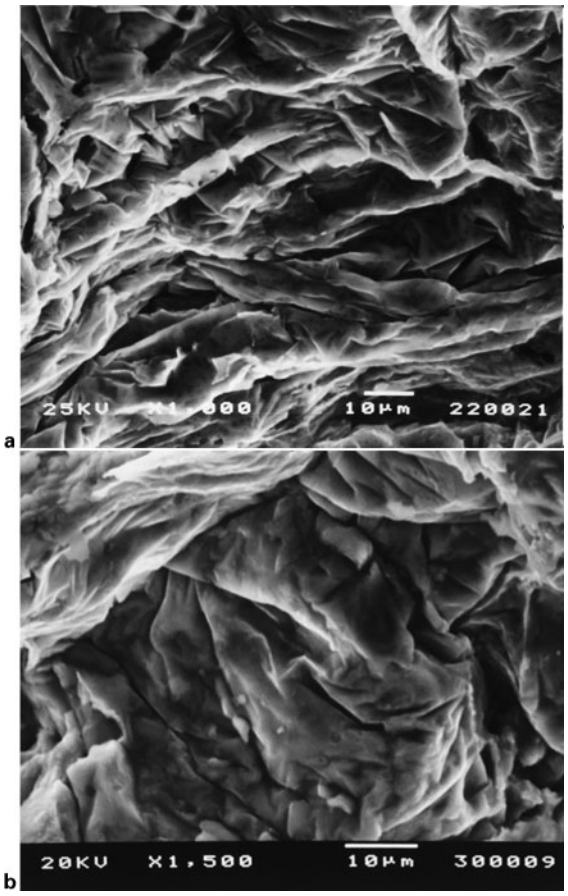

1 Images (SEM) showing *a* new and *b* old oxide film on fracture surface of Al–7Si–Mg casting[12]

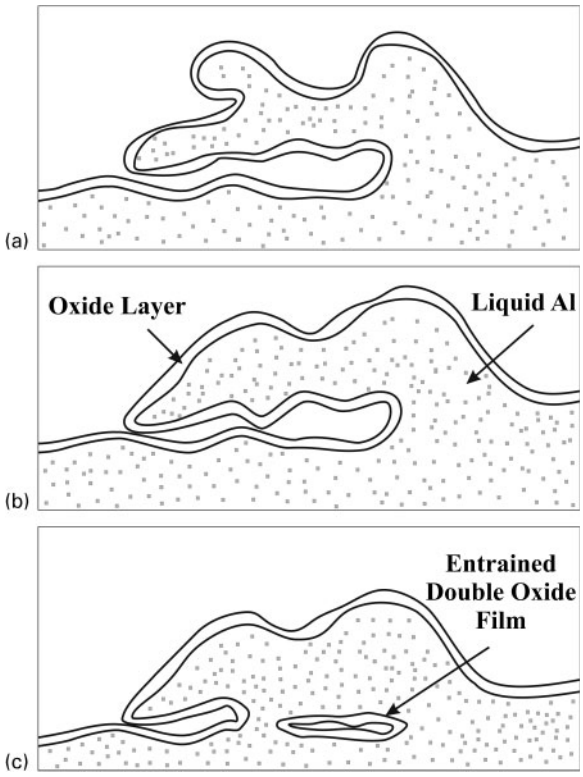

2 Schematic showing entrainment of double oxide film defect, *a* surface turbulence, *b* formation of bifilm having two unwetted sides of oxide films contacting with each other and *c* double oxide film–bifilm that is submerged in bulk of liquid acting as cracks[9]

coverall flux (Foseco 110). No additional treatment was performed on the melt. Following the pouring of molten metal into a simple cylindrical shape casting via bottom gating system, a steady succession of bubbles was artificially introduced via a silica tube into the base of the casting. If an air bubble was trapped by solidifying metal, the subsequent bubble might collide with it. The contacting region between the bubbles was separated from casting as OMO sandwich and examined by SEM. A schematic drawing of the air blowing system, a three-dimensional view of the contact area between two bubbles and the cross-view of OMO sandwich are shown in Fig. 4.

Results and discussion

Figure 5*a* shows an OMO sandwich inside a casting of pure aluminium quite similar to Fig. 4*b*. According to previous studies, new oxide films on the sandwich are sufficiently thin so that the dendrite structure can be seen (note that the oxide film covers both side of the sandwich).[15–18] Three different regions are labelled as A, B and C in Fig. 5*a*. In region A, the tips of dendrites are visible underneath the draped oxide film. Region B is another part of OMO sandwich in which two oxide layers are matched in such a way that no solidified melt is possibly remained in between. Region C shows another part of OMO sandwich that is similar to region B but is broken during sample preparation. It has to be noted that during sample preparation, one has to cut the casting very close to the bubbles that remained in the solidified melt; therefore, vibration of the cutter may cause breaking of the oxide film, which is naturally a brittle material. A cross-view of the depicted section in Fig. 5*a* is shown schematically in Fig. 5*b*.

Figure 6*a* shows another part of OMO sandwich. This is the area at the upper left side of the region, labelled as C in Fig. 5*a*, but has been turned down during SEM image taking. In the area labelled as D, a dendrite arm with some secondary arms has been separated and isolated from bulk metal as a result of melt volume contraction. A closer view of region D is shown in Fig. 6*b*, in which dendrite arms are clearly visible while a layer of folded oxide film has covered them. Overall length of the dendrite shown in this figure is nearly 150 μm. Other features of interest, in this figure, are the dimensions of secondary arms, presence of a double film layer shown as white areas and crack that is visible in the areas labelled as E and F.

Figure 6*c* shows more details of the area labelled as E. As seen in this figure, the whole surface is covered with the folded oxide film. The thickness of the folding perpendicular to the surface is in the range of 0·3–0·8 μm. Isolated drops of solidified melt can be seen through the thin oxide film in the lower left hand side of the figure. Three tears are visible in the upper right side of the image, which seem to be the result of brittleness of the oxide film and stresses induced during sample preparation. It seems that on the surface of the oxide film, especially on the lower right side of the image, some grains have started to grow. This is possibly the next step in the growth of oxide film, which needs to be investigated with proper equipment in the future. The size of the tips of the dendrite is in the range of 15–20 μm. An isolated

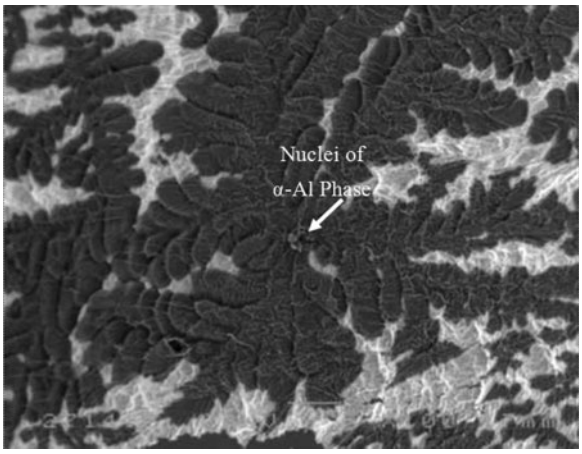

3 Oxide–metal–oxide sandwich taken from Al–5Mg alloy showing inoculation site of α phase[16]

solidified melt having a needle-like shape in the upper right hand side of the image is visible.

Figure 6*d* shows a close view of region F in Fig. 6*b*. According to this image, folds along the stressful areas of solidified and isolated droplets are thicker than other folds in the bright areas. At least four isolated droplets are visible in this image. A main crack, which has started from the edge, continued to the left side of the image, while a small crack is also visible above it.

Another OMO sandwich formed in pure aluminium is shown in Fig. 7. Dendrite tips of the solidified melt, which are covered by the folded oxide film, are clearly seen similar to other figures. In the central bright area, two oxide layers from each bubble are matched due to the lack of melt, which has been extracted toward surroundings dendrites. Figure 7*b* shows the central bright area at higher magnification. Wrinkles that exist in Fig. 7*b* are mostly thinner than 1 μm.

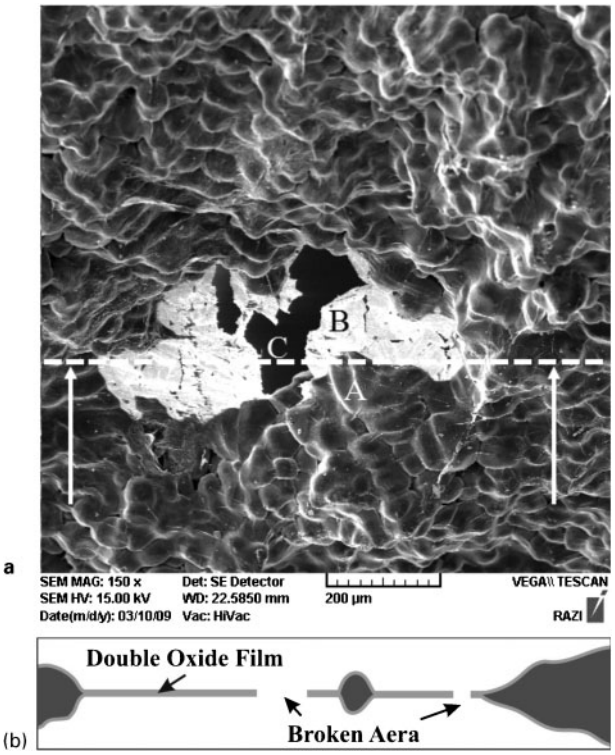

5 *a* image (SEM) showing OMO sandwich, taken from contact area between two entrapped bubbles in pure aluminium and *b* schematic cross-view of sandwich

Solidification behaviour of sandwich

The last volume of the melt between two collided bubbles tends to move circularly out toward reminded melt from the contact area. However, the buoyancy force of the lower bubble is not able to create such a strong force to push the melt totally out of the contact area. If the collided bubbles are produced by air

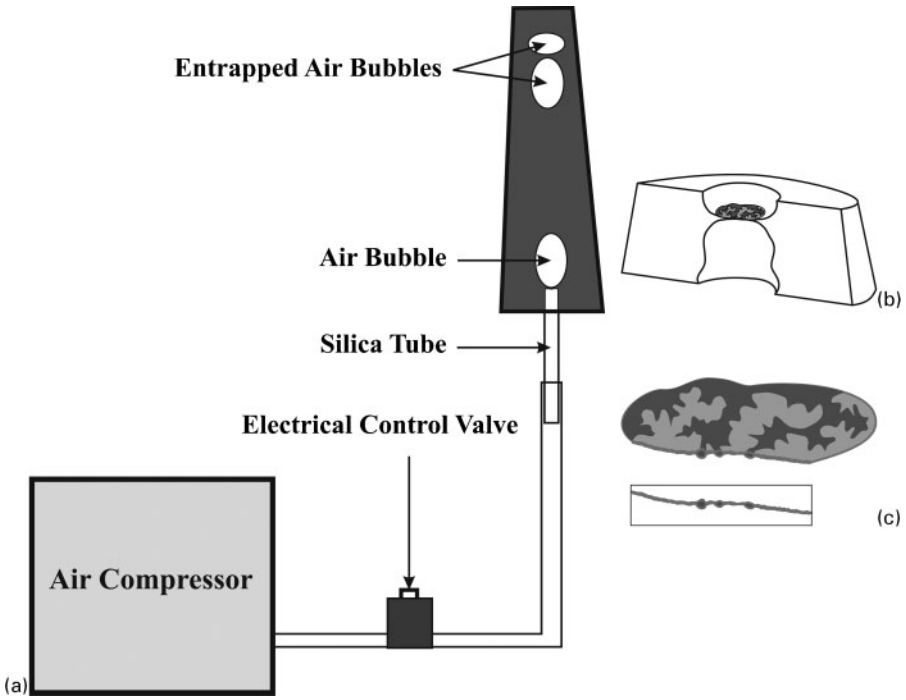

4 Schematic illustration of *a* air blowing system, *b* three-dimensional view of collided bubbles and their interface named as OMO sandwich sample and *c* top and cross-section view of OMO sandwich

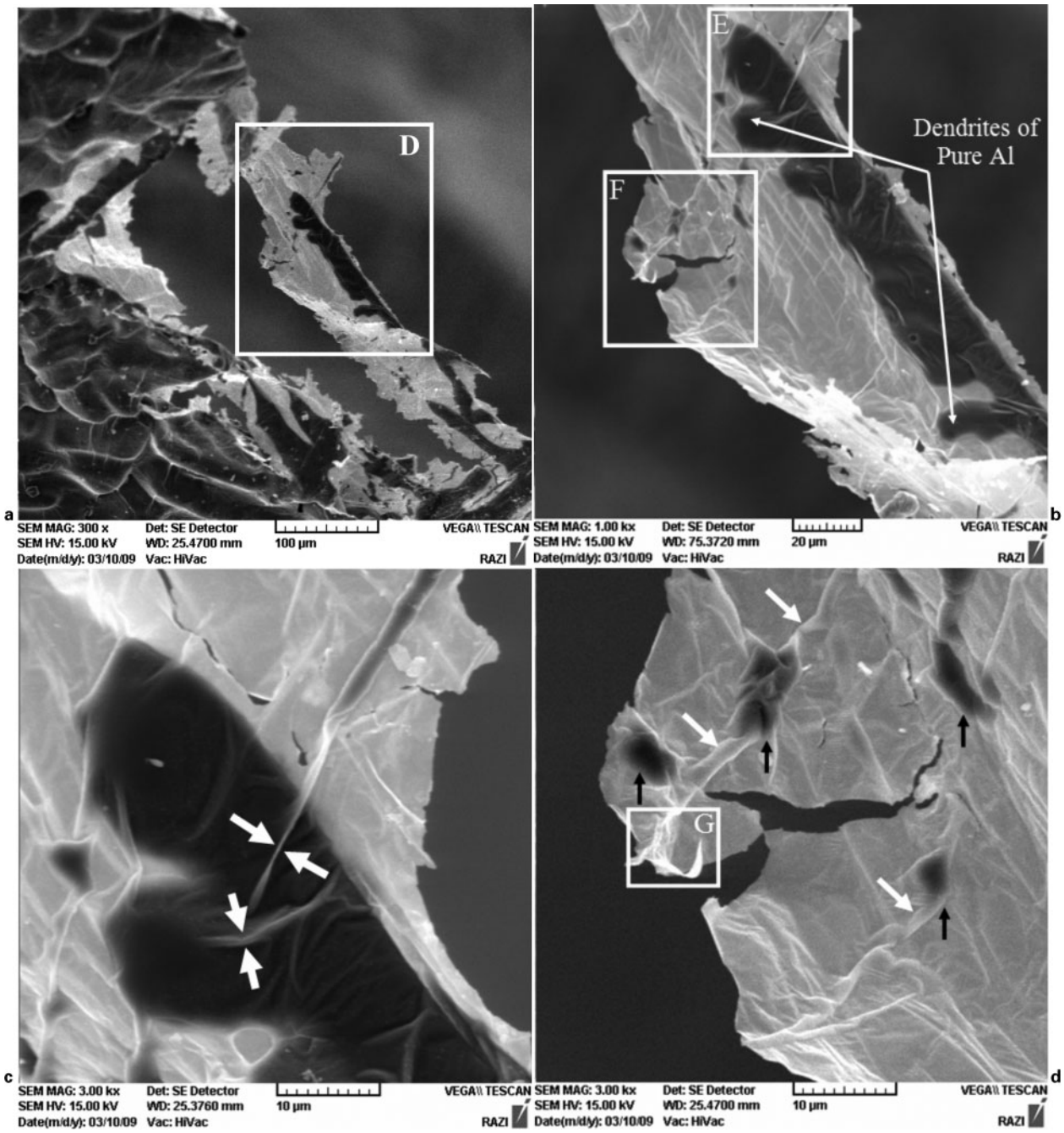

6 *a* part of OMO sandwich in pure aluminium, *b* closer view of region D showing dendritic growth of melt, *c* region E in *b* at higher magnification showing oxide folds and *d* close view of region F in *b* that shows dispersed and isolated solidified droplets and cracked double oxide film

injection, one has to expect an oxide film to be present in each side of the narrow layer of the somehow encapsulated melt, which is <10 µm thick, in most cases.[15–18] This is the condition in which the OMO sandwiches are created as shown in Fig. 8*a*. Following this stage, solid nuclei start to form inside the sandwich (Fig. 8*b*). Then, the dendrites of solidifying and growing nuclei cause the surrounding melt atoms to start to move toward them (Fig. 8*c* and *d*). The volume contraction of the melt causes the oxide films of the upper and lower sides of the OMO sandwich to be sucked toward the centre core of the sandwich. Figure 8*e* shows this stage. If in some places two layers of the oxide film are touched, as a result of melt displacement, then the oxide film thickness in such areas is twice the oxide film of each side. This means that if one looks at the OMO sandwich by SEM from the edge, it would be possible to measure oxide film thickness as has been reported.[16]

Returning now to the other characteristic of OMO sandwich, it is worth mentioning that analysing the composition of the nucleation site is possible using proper equipment because of the visibility of the position of the nuclei inside the sandwich.[15–17] In most cases, the sizes of the dendrites are between 30 and 70 µm, but the thickness of the sandwich is nearly 10 µm, which causes dendrites to be flattened parallel to the oxide film layers.

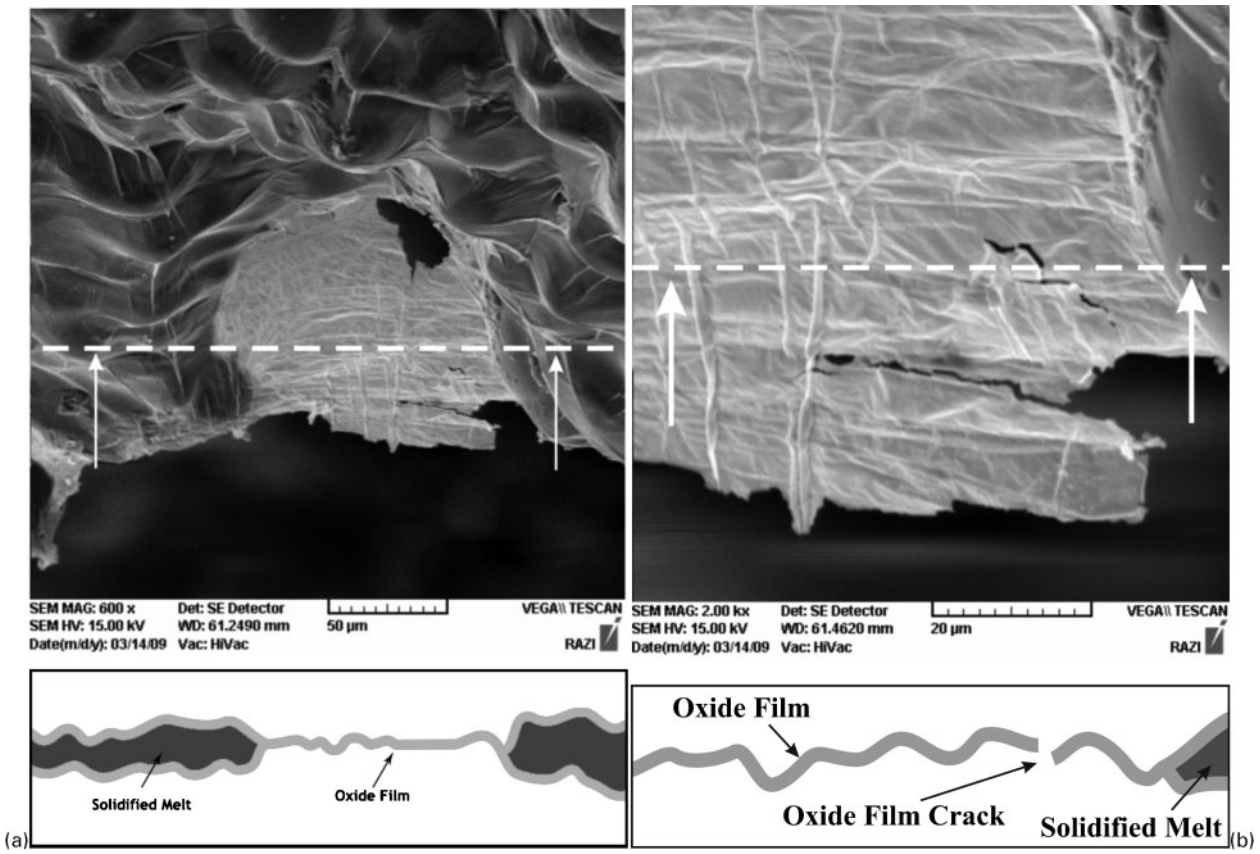

7 ***a*** **wrinkles on dendrite tips and its schematic cross-section and** ***b*** **same image at higher magnification, showing folded feature of short time oxide films**

Oxide film folding

Oxide film folding may occur in both cases, above and below the solidus temperature. Therefore, folds seen in the oxide films can be categorised in two groups: (i) those that form above the solidus temperature and fall into two groups including folds and wrinkles and (ii) those that form below the solidus and are only in wrinkle-like forms (Fig. 9).

Folds formed above solidus temperature

For an alumina film on the surface of liquid aluminium, the underside of the film is in perfect atomic contact with the melt. It means that the surface oxide film can be considered as well as wetted by the melt. Thus, the surface oxide film can be affected by melt turbulence stresses. For relaxing from turbulence stress, the surface oxide film deforms and folds. This type of folding that appears thicker than other types is named fold (Fig. 2).

According to Fig. 10, the difference between contraction coefficient of molten aluminium and solid oxide aluminium is more than twice at 1000 K. Such a difference is able to create a contraction stress, and the result can fold the oxide film. This sort of deformation and the resulting fold can be called wrinkle (Fig. 11).

Folds formed under solidus temperature

As solidifying goes on, in addition to contraction stress, the surface oxide film of an OMO sandwich is subjected to stress due to the suction of melt toward the solid nuclei. These stresses and dendritic growth of the melt lead to another type of folds called wrinkle, which form on the tips of the dendrites. All types of the short time oxide film folds are shown in Fig. 12. There are also some cracks in this figure, which are typical in most images taken from the sandwiches. It is worth mentioning that the aluminium oxide layer is a ceramic and therefore is a brittle material. However, it can be deformed due to the contraction stress, especially in high temperature. Obviously, if the stress rises above its strength, it will crack.

Thickness estimation

In previous studies, the oxide film thickness has been estimated based on two methods: (i) using SEM image taken from the edge of OMO sandwich[15] and (ii) using folds as a criteria for film thickness estimation.[18] However, estimating film thickness by halving the measured thickness of folds may seem to oversimplify and possibly overestimate the thickness of the film. The overestimation is compounded by the additional melt trapped inside the folds and partly from the residual rigidity of the films that helps it to resist conformance to a sharp bend (Fig. 13). However, comparison of various alloys' oxidation behaviours can be performed by this method.

The results of measurements of 'fold thickness' in this research and other reports[15–17] are presented in Fig. 14. According to this figure, by increasing magnesium content in aluminium alloys, fold thickness (especially the minimum of fold thickness) is increased. It seems that, among researchers, it is generally accepted that the oxide film thickness depends on magnesium content in aluminium alloys.[1,2,5,16] Therefore, it is expected that increasing magnesium content in these alloys resulted in

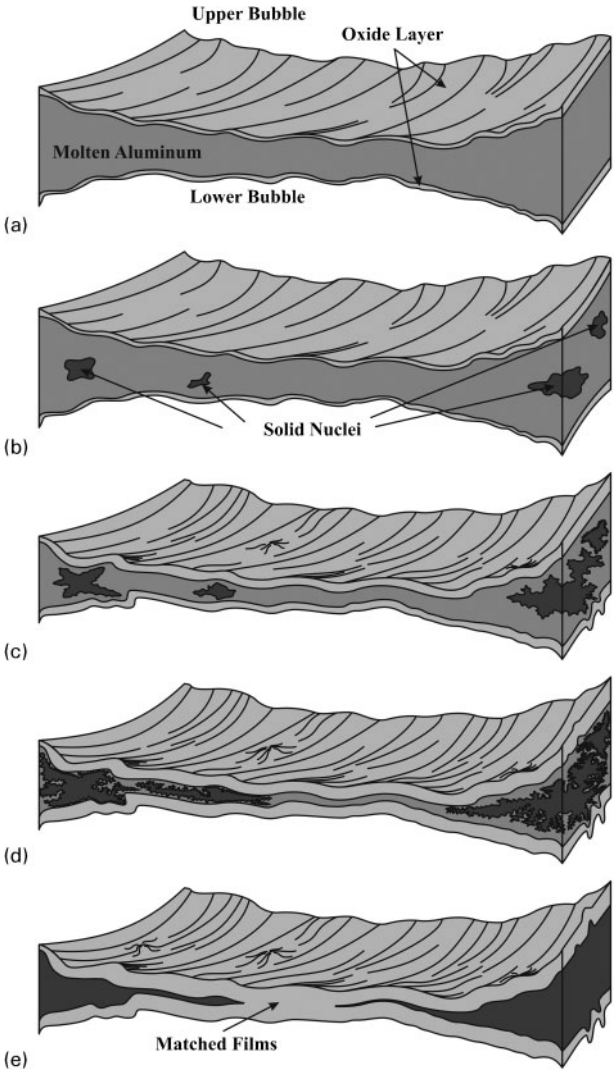

8 Schematic illustration of *a* entrapped melt between two oxide layers (OMO sandwich), *b* solid nucleation in melt, *c* beginning of dendritic growth, *d* melt suction toward solid nuclei and *e* solidified OMO sandwich; note oxide films matching in region possibly free from metal

the increase in minimum fold thickness. Based on the low differences between the minimum values of fold thickness in pure aluminium and in Al–7Si–0·4Mg alloy, it seems that silicon cannot affect the oxide film thickness in aluminium alloys. This finding is in agreement with other researchers' report.[1,13]

Conclusions

1. Folds occur before solidification due to the melt flow stress. Some wrinkles form before solidification due to contraction stress, and some of them are produced during solidification on dendrites tips.

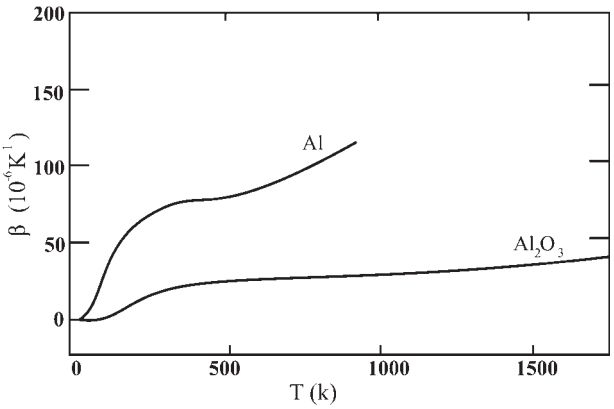

10 Cubic expansion coefficient β (T) of aluminium and aluminium oxide as function of temperature[8]

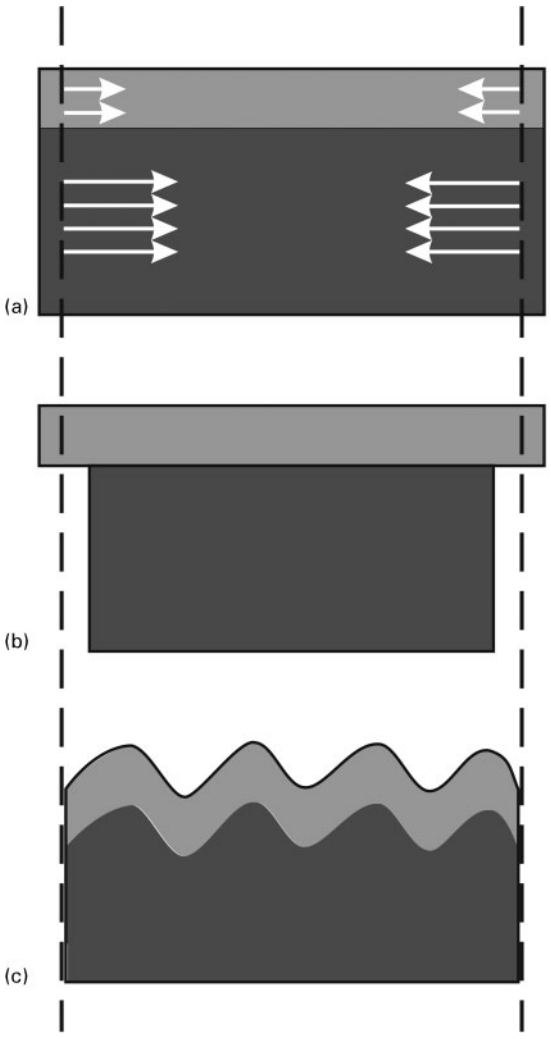

11 Schematic drawing showing *a* lower contraction stress exerted on oxide film than melt, *b* contraction of oxide film and melt not regarding wetting of oxide film and melt and *c* oxide film folding to free from contraction stress and wrinkle formation regarding wetting

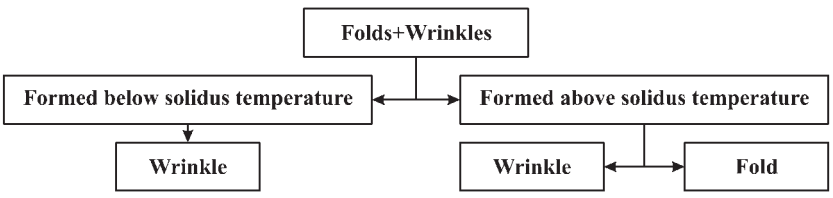

9 Classification of fold types that may form during short time oxidation

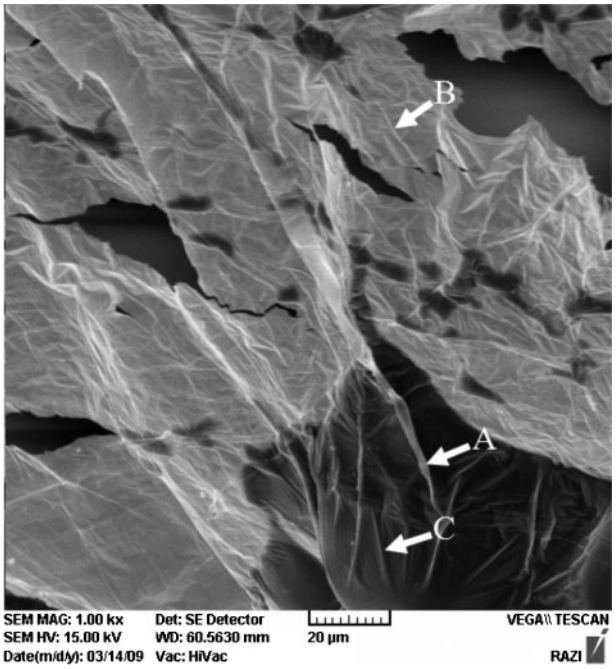

12 Types of folds including *a* fold, *b* wrinkle formed before solidification and *c* wrinkle formed during solidification

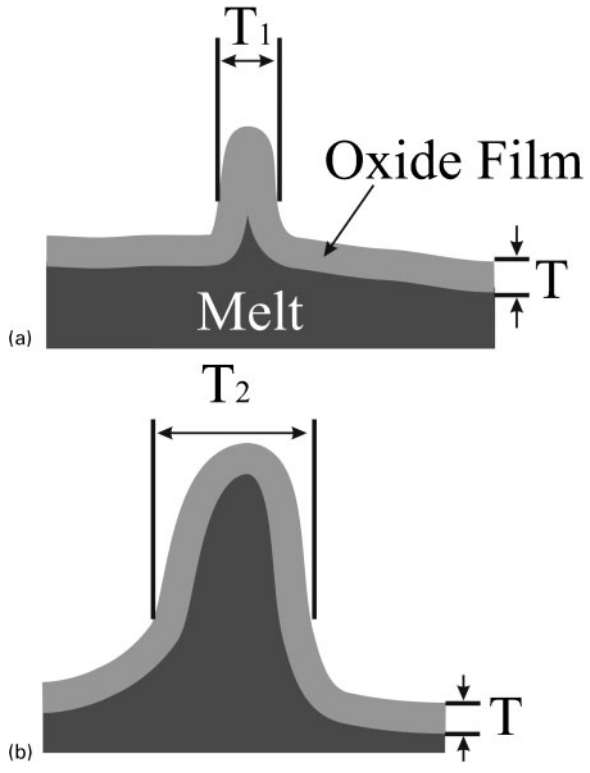

13 Effect of entrapped material between oxide layers on fold thickness, $T_1 < T_2$

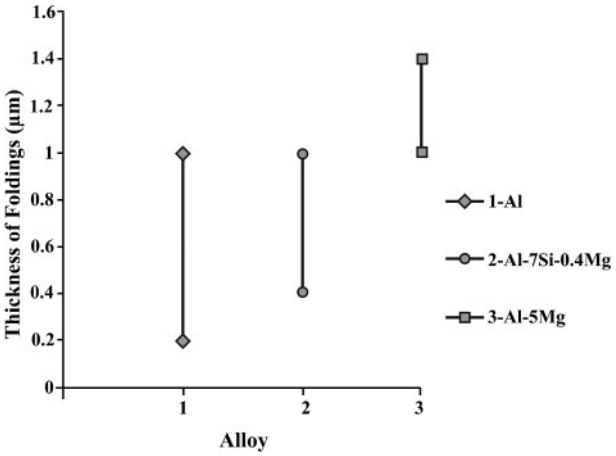

14 Measured fold thickness in three different aluminium alloys

2. Minimum value of the fold thickness is measured ~200 nm, so the thickness of short time surface oxide film is ~100 nm in pure aluminium.

3. Regions of OMO sandwich that are bright in the SEM images might become a single oxide layer as a result of melt suction from these regions.

References

1. W. Thiele: *Aluminium*, 1962, **38**, 707–715.
2. C. N. Cocharn, D. L. Belitskus and D. L. Kinosz: *Metall. Trans. B*, 1977, **8B**, 323–332.
3. K. Shimizu, G. M. Brown, K. Kobayashi, G. E. Thompson and G. C. Wood: *Corros. Sci.,* 1993, **34**, 1853.
4. E. Bergsmark, C. J. Simensen and P. Kofstad: *Mater. Sci. Eng. A*, 1989, **120A**, 91–95.
5. G. Wightman and D. J. Fray: *Metall. Trans. B*, 1983, **14B**, 625–631.
6. A. Guppy, A. J. Wickens and D. J. Fray: *Trans. IMM*, 1972, **81**, 236–242.
7. G. Wightman and D. J. Fray: *Trans. IMM*, 1982, **91**, 123–128.
8. G. Grimvall: 'Thermophysical properties of materials'; 1999, Amsterdam, Elsevier Science B.V.
9. R. Raiszadeh and W. D. Griffiths: *Metall. Mater. Trans. B*, 2006, **37B**, 865–871.
10. N. R. Green and J. Campbell: *AFS Trans.*, 1994, **102**, 341–347.
11. C. Nyahumwa, N. R. Green and J. Campbell: *AFS Trans.*, 1998, **106**, 215–223.
12. C. Nyahumwa, N. R. Green and J. Campbell: *Metall. Mater. Trans. A*, 2001, **32A**, 349–358.
13. J.Campbell: 'Castings', 2nd edn; 2003, Oxford, Butterworth-Heinemann Pub. Co.
14. J. Campbell: *Mater. Sci. Technol.*, 2006, **22**, (2), 127–145.
15. M. Divandari and J. Campbell: *Aluminum Trans.*, 2000, **2**, 233–238.
16. M. Divandari and J. Campbell: *Int. J. Cast Met. Res.*, 2005, **18**, (3), 1–6.
17. M. Divandari and J. Campbell: *Int. J. Cast Met. Res.*, 2004, **17**, (3), 1–6.
18. A. R. Mirak, M. Divandari, S. M. A. Boutorabi and J. Campbell: *Int. J. Cast Met. Res.*, 2007, **20**, (4), 215–220.